ACS APPLIED MATERIALS & INTERFACES

Research Article

www.acsami.org

Physically Adsorbed Fullerene Layer on Positively Charged Sites on Zinc Oxide Cathode Affords Efficiency Enhancement in Inverted Polymer Solar Cell

Yu-Shan Cheng, Sih-Hao Liao, Yi-Lun Li, and Show-An Chen*

Chemical Engineering Department and Frontier Research Center on Fundamental and Applied Sciences of Matters, National Tsing-Hua University, No. 101, Section 2, Kuang-Fu Road, Hsinchu, Taiwan, 30013, Republic of China

ABSTRACT: We present a novel idea for overcoming the drawback of poor contact between the ZnO cathode and active layer interface in an inverted polymer solar cell (i-PSC), simply by incorporating an electron-acceptor self-assembled monolayer (SAM)—tetrafluoroterephthalic acid (TFTPA)—on the ZnO cathode surface to create an electron-poor surface of TFTPA on ZnO. The TFTPA molecules on ZnO are anchored on the ZnO surface by reacting its carboxyl groups with hydroxyl groups on the ZnO surface, such that the tetrafluoroterephthalate moieties lay on the surface with plane-on electron-poor benzene rings acting as positive charge centers. Upon coating a layer of fullerenes on top of it, the fullerene molecules can be physically adsorbed by Coulombic interaction and facilitate a promoted electron collection from the bulk. The active layer is composed of the mid bandgap polymer poly(3-hexylthiophene) (P3HT) or low bandgap polymer, poly[[4,8-bis[(2-ethylhexyl)oxy]benzo[1,2-*b*:4,5-*b*′]dithiophene-2,6-diyl][3-fluoro-2-[(2-ethylhexyl) carbonyl]thieno[3,4-*b*]-thiophenediyl]] (PTB7), as the donor and [6,6]-phenyl-C_{61}-butyric acid methyl ester ($PC_{61}BM$) or [6,6]-phenyl-C_{71}-butyric acid methyl ester ($PC_{71}BM$) as the acceptor. Significant enhancement in power conversion efficiency (PCE) was observed for the devices with the active layer P3HT:$PC_{61}BM$ (or $PC_{71}BM$) by promoting from 3.20 to 4.03% (or from 3.27 to 4.04%) and with the active layer PTB7:$PC_{71}BM$ from 6.03 to 6.90%. This method should be also applicable to other types of active layer.

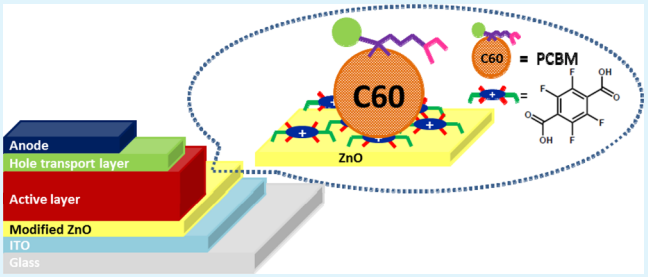

KEYWORDS: *polymer solar cell, self-assembled monolayer, interface, fluorobenzene, fullerene*

INTRODUCTION

Bulk-heterojunction (BHJ) polymer solar cells[1] (PSCs) with an active layer composed of a conjugated polymer as the donor and a fullerene derivative as the acceptor have attracted great attention because of their ease of fabrication, promising flexibility, and capability for large-scale and low-cost production. Poly(3-hexylthiophene) (P3HT) with high regioregularity and [6,6]-phenyl-C_{61}-butyric acid methyl ester ($PC_{61}BM$) are the most representative conjugated polymer donor material and acceptor material, respectively. PSCs based on these two materials can reach the power conversion efficiencies (PCEs) of 4−5%.[2] One way to enhance the PCE by changing the active layer is to design an acceptor with a higher lowest unoccupied molecular orbital (LUMO) level for increasing V_{oc}, such as indene−PCBM (IPCBM)[3] and indene−C_{60} bisadduct (ICBA).[4] The other way is to replace P3HT with lower-bandgap polymers,[28−30] allowing a promotion of PCE from 5 to over 7%, as reported for the donors such as thieno[3,4-b]thiophene/benzodithiophene (PTB7) along with the fullerene derivative acceptor [6,6]-phenyl-C_{71}-butyric acid methyl ester ($PC_{71}BM$).[5−7] Other than material design for the active layer, the insertion of an electron transport layer (ETL) between the active layer and metal cathode can also increase its PCE. For examples, insertion of the water or alcohol-soluble ETLs based on polyfluorene grafted with *N*,*N*-dimethylamino (PFN)[8] promoted PCE from 7.13% to 8.37% and that with crown ether (PFCn6)[9] from 5.78% to 7.5%.

In a conventional PSC, an active layer composed of polymer donor and acceptor material is sandwiched between transparent conducting indium tin oxide (ITO) and low work function metal electrode, by which holes and electrons are collected, respectively. However, prolonged exposure of this kind of device to air can lead to oxidation of the air-sensitive metal electrode, resulting in degradation of performance.[10] In order to alleviate this problem, the reverse of device architecture, the inverted PSC (i-PSC), is employed,[11−13,31−34] in which a less air-sensitive high work function metal (Ag, Au) is used as the back hole collecting electrode and ZnO or TiOx is used as the electron collecting interlayer between ITO and active layer.[12,14,32−34] However, such inorganic electron collecting interlayer could lead to a poor interfacial contact with organic active layer and result in a poor electron extraction.[15] Thus, interface modification becomes an important issue for improving electron extraction. For doing so, fullerene derivatives were used for the interface modification in order to reduce the possibility for electron quenching at the interface.

Received: April 19, 2013
Accepted: June 24, 2013
Published: June 24, 2013

The fullerene-derivative, fullerene-end-capped poly(ethylene glycol) (PEG-C60),[16] blended into the active layer composed of P3HT and $PC_{61}BM$ as the additive in normal type solar cell can produce a fullerene-rich interface in between the metal cathode and active layer and result in an increase of PCE from 3.6% to 4.4%. The cross-linkable fullerene derivative, [6,6]-phenyl-C_{61}-butyric styryldendron ester (PCBSD),[15] as the electron transport layer provided an improvement in PCE of the i-PSC with P3HT:$PC_{61}BM$ as the active layer from 3.5% to 3.68−4.4%. Alternatively, an incorporation of a self-assembled monolayer (SAM) of fullerene derivatives[17] on the ZnO surface was also used, which provided the improved PCE from 3.47% to 4.4%. All the cases above present the importance of surface modification and the necessity of producing a fullerene-rich interface between the active layer and metal oxide in an i-PSC.

Multifluorine substituted benzene has its nature of electron-depleted ring center since the electron-withdrawing characteristics of the F substituents make electron density move towards F atoms in the periphery. The more positive electrostatic potential carbon ring is in contrast with the high electron density of nonsubstituted benzene. Thus, multifluorine substituted benzene owns the capability to strongly interact with electron-rich species such as double bonds and aromatic rings.[18−21] Here, we present a novel idea for efficient collecting electrons to ZnO cathode by modifying its surface with plane-on tetrafluoroterephthalate as positive charge sites and subsequently allowing the fullerene derivative to adsorb on the surface via Coulombic interaction by spin-coating from its solution and then washing with solvent. Such treatment can prevent a direct contact of the polymer donor in the active layer with ZnO and therefore reduce the chance of electron recombination with holes at the interface, thus an enhancement in PCE results. For all the devices investigated with active layers—mid bandgap polymer P3HT with $PC_{61}BM$ or $PC_{71}BM$ and the low bandgap polymer PTB7 with $PC_{71}BM$—the current density is improved by about 1.5−2 mA cm^{-2} and the PCE improves by about 0.9%.

EXPERIMENTAL SECTION

Materials. Regioregular poly(3-hexyl-thiophene) (P3HT, 4002-Egrade, regioregularity 97.8%) from Rieke Metals, Inc. and PTB7 from One Material were used without further purification. [6,6]-Phenyl-C_{61}-butyric acid methyl ester ($PC_{61}BM$) and [6,6]-phenyl-C_{71}-butyric acid methyl ester ($PC_{71}BM$) from Nano-C (99.5% purity), 1,2-dichlorobenzene (ODCB) from Alfa-Aesar (99.0% purity), chlorobenzene (CB) from J. T. Baker (99.0% purity), 1,8-diodooctane from Sigma-Aldrich (98.0% purity), 2,3,5,6-tetrafluoro-1,4-benzenedicarboxylic acid (TFTPA) from Sigma-Aldrich (97% purity), 2,3,4,5,6-pentafluorobenzoic acid (PFBA) from Sigma-Aldrich (97% purity), and terephthalic acid (TPA) from Sigma-Aldrich (99% purity) were used also without further purification.

General Measurements, Device Fabrication, and Characterization. Characterization on various ZnO surfaces before and after treatments were performed with water drop as the probe using contact angle meter (GBX DIGIDROP). X-ray photoelectron spectroscopy (XPS) and ultraviolet photoelectron spectroscopy (UPS) (VG, MULTILAB 2000) under a base pressure of 1×10^{-9} mbar using monochromatized Mg (Kα) X-rays ($h\nu$ = 1254.6 eV) and He I ultraviolet light ($h\nu$ = 21.2 eV) as light source in XPS and UPS, respectively. The HOMO level is determined from the results of UPS along with the equation, HOMO level = $h\nu - (E_{cutoff} - E_{onset})$, where $h\nu$ is incident photon energy (21.2 eV) of He I, E_{cutoff} is the high binding energy cutoff and E_{onset} is the binding energy in HOMO region taking at the turning points. The E_{cutoff} is determined by linear extrapolation to zero at the yield of secondary electrons, and the E_{onset} is the onset relative to the Femi level (E_f) of Au (0 eV), where the E_f is determined from the Au substrate. And, the LUMO level is determined by the equation, LUMO level = highest occupied molecular orbital (HOMO) level − optical band gap, where optical band gap of ZnO is 3.10 eV.[22]

For the i-PSC fabrication, thin film of ZnO was prepared by the procedure similar to that reported previously,[23] in which ZnO precursor solution was spin-cast at 5000 rpm on top of a cleaned ITO and, then, sintered at 200 °C for 1 h in air, resulting in transparent ZnO thin film with the thickness about 40 nm. The ZnO precursor solution was prepared by dissolving zinc acetate dehydrate ($C_4H_6O_4Zn{\cdot}2(H2O)$) 99.5% from Merck, 1 g) and monoethanolamine ($HOCH_2CH_2NH_2$, 98% from Acros, 0.282 g) in 2-methoxyethanol (10 mL) under stirring for 8 h for hydrolysis reaction and aging. Then the ZnO film on ITO is soaked into 0.1 mM self-assembled monolayer solution (TFTPA and PFBA are dissolved in ethyl acetate while the TPA is dissolved in dimethyl sulfoxide) for 10 min at room temperature and then washed with clean solvent (the same solvent as in the corresponding solution). On top of the modified-ZnO or pristine ZnO, a thin layer (about 100 nm) of P3HT:$PC_{61}BM$ (or $PC_{71}BM$) (1:1, w/w) in 1,2-dichlorobenzene or PTB7:$PC_{71}BM$ (1:1.5, w/w) in the mixed solvent (chlorobenzene/1,8-diiodooctane, 98:2 v/v) was spin-cast in argon-filled glovebox and dried in covered glass Petri dish for 2 h in P3HT-based devices. The devices were then moved to atmosphere and then spin-coated with PEDOT:PSS (Clevios P VP AI4083) onto the P3HT:$PC_{61}BM$ (or $PC_{71}BM$) film as the hole transport layer (HTL) (about 60 nm) and dried for 10 min at 120 °C. In order to improve the wettability of PEDOT:PSS above, the surfactant triton X-100 (laboratory grade, Sigma-Aldrich) was added to its aqueous solution such that the weight ratio of solid PEDOT:PSS to triton X-100 is 1.5. In the PTB7−$PC_{71}BM$ system, a thin layer of MoO3 (about 10 nm) was thermal deposited as the HTL. Finally, a layer of Ag (100 nm) as the anode was thermally deposited through a shadow mask at a pressure of less than 2×10^{-6} Torr. The active area of the device is about 7.5 mm^2.

The current−voltage (J−V) characteristics of the unencapsulated i-PSCs were measured in air using a Keithley 2400 source-measure unit and an AM 1.5 G solar simulator (Oriel 94021A, 150 W from Newport). The illumination intensity of 100 mW cm^{-2} irradiation was calibrated using a standard monocrystal Si reference cell (Oriel 91150 V from Newport) to ensure the accurate light source intensity. The same data acquisition system was used for the external quantum efficiency (EQE) measurement. Under full computer control, light from a 150 W xenon lamp (Oriel, U.S.A.) was focused through a monochromator onto the PSC under testing. The wavelength of the light from the monochromator was incremented in the visible region to generate the EQE (λ) as defined by EQE (λ) = 12 400($J_{sc}/\lambda\varphi$), where λ is the wavelength, J_{sc} is the short-circuit photocurrent density (mA cm^{-2}), and φ is the incident radiative flux (mW cm^{-2}). J−V characteristics and EQE of the unencapsulated PSCs were measured in air.

RESULTS AND DISCUSSION

Contact Angle Measurement on Treated and Pristine ZnO Surfaces. In order to examine if the SAM of fluorobenzene derivatives is able to physically adsorb $PC_{61}BM$, we choose two different molecules, TFTPA and pentafluorobenzoic acid (PFBA), as candidates, which contain two and one carboxylic acid groups, respectively. The SAM was prepared by first soaking ZnO into 0.1 mM TFTPA (or PFBA) solution for 10 min to allow its −COOH groups of SAM reacting with −OH groups on ZnO surface,[24] resulting in plane-on positive charge sites of tetrafluoroterephthalate (or edge-on positive sites of fluorobenzoate) on the ZnO surface. As the contact angle measurement with a water drop as the probe shows (see Figure 1), the TFTPA-modified ZnO (TFTPA-ZnO) (21.9°) becomes more hydrophilic than pristine ZnO (40.4°); while the PFBA-modified ZnO

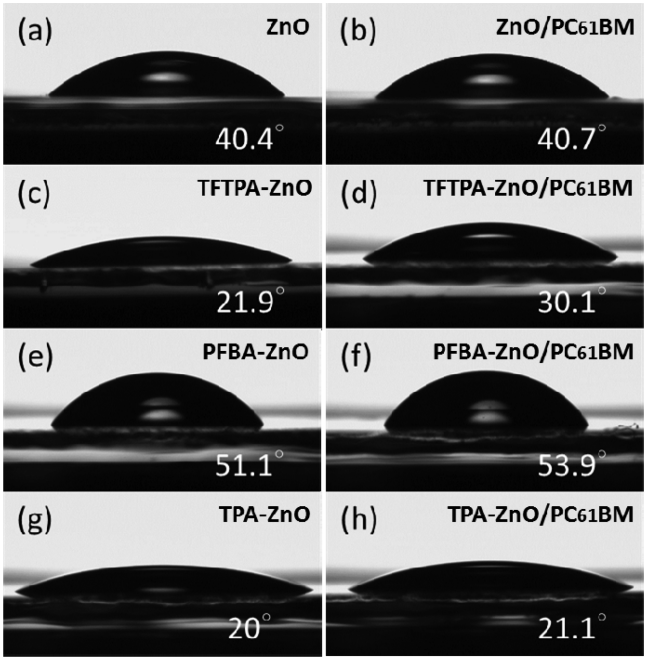

Figure 1. Contact angles with deionized (DI) water drops on the modified ZnO with different SAMs without and with $PC_{61}BM$ precoating, which were prepared by spin-coating a layer of $PC_{61}BM$ from its solution in chlorobenzene and then washing with chlorobenzene, designated as "/$PC_{61}BM$". (a) Pristine ZnO; (b) ZnO/$PC_{61}BM$; (c) TFTPA–ZnO; (d) TFTPA–ZnO/$PC_{61}BM$; (e) PFBA–ZnO; (f) PFBA–ZnO/$PC_{61}BM$; (g) TPA–ZnO; and (h) TPA–ZnO/$PC_{61}BM$.

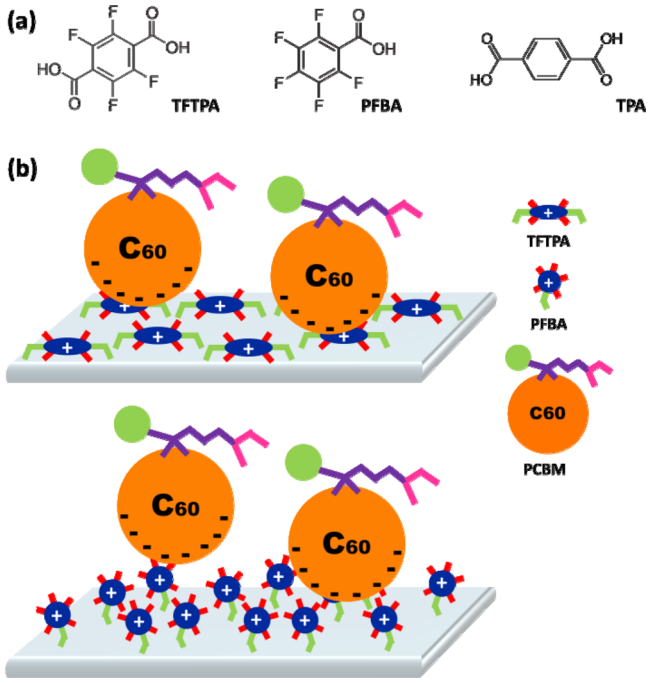

Figure 2. (a) Chemical structures of tetrafluoroterephthalic acid (TFTPA), pentafluorobenzoic acid (PFBA), and terephthalic acid (TPA). (b) Schemes of the interactions between fluorobenzene ring and $PC_{61}BM$. The upper scheme shows the plane-on orientation of TFTPA having the electron-favorable center of fluorobenzene laying on the ZnO surface which is in contact with $PC_{61}BM$ effectively; the lower scheme shows the edge-on (vertical orientation) of PFBA having the electron-rich fluorine substituents exposed to the ZnO surface which is much more difficult to adsorb $PC_{61}BM$.

(PFBA–ZnO) (51.1°) becomes more hydrophobic indicating the different molecular orientations on ZnO surface of these two SAMs. PFBA would tend to bond to ZnO with the fluorobenzene ring oriented vertically to ZnO surface since only one reactive site −COOH on it.[25] Thus, its fluorine substituents would expose at the outmost surface of the SAM and form a very low free energy surface, which is the main reason for hydrophobic characteristic in PFBA-ZnO. Whereas TFTPA owns two −COOH reactive sites at the para-position of its fluorobenzene ring, both sites would bond on to ZnO surface and therefore cause the fluorobenzene ring to be oriented parallel (plane-on) to the ZnO surface.[25] The hydrophilic characteristics of TFTPA–ZnO can be attributed to the two reasons below. First, it is plane-on orientation allows the two ester groups to be exposed at the outmost place. Second, the fluorobenzene ring center of TFTPA is electron depleted resulting in four strong electron withdrawing fluorine-substituents, which is able to attract the lone pair electron on the oxygen of water.

To test the capabilities of these two types of SAMs of attracting fullerene derivatives, we spin-coated a layer of $PC_{61}BM$ from its solution in chlorobenzene on the modified- and unmodified-ZnO surface and then washed away the nonadsorbed residue with chlorobenzene. We then examined if significant a amount of $PC_{61}BM$ was adsorbed on the modified surface by contact angle measurement. As can be seen from Figure 1, only the TFTPA–ZnO gives obvious change (21.9° → 30.1°) while the PFBA–ZnO and pristine ZnO give only slight change (51.1° → 53.9° and 40.4° → 40.7°). These indicate that the plane-on orientation of TFTPA is able to attract $PC_{61}BM$ (see Figure 2b upper one); while in the case of PFBA, the positive center of fluorobenzene ring is perpendicular to the ZnO surface and can interact with $PC_{61}BM$ molecule only if its neighboring vicinity is empty able to accommodate one as shown in the bottom of Figure 2b. Furthermore, to ensure that $PC_{61}BM$ is adsorbed by the positive center of fluorobenzene, we replace TFTPA with the similar molecule without any fluorine substitution, terephthalic acid (TPA), to undergo same modification on ZnO and then test for its contact angle. TPA-modified ZnO (TPA–ZnO) after spin-coated with $PC_{61}BM$ and then washing with solvent gives only slight change (20° → 21.1°), which further support the fact that the plane-on tetrafluoroterephthalate bonded on ZnO surface provides positive charge center and able to absorb $PC_{61}BM$.

X-ray Photoelectron Spectroscopy (XPS) Measurement on Treated and Pristine ZnO Surfaces. We carry out the elemental analysis on the surfaces of the treated and pristine ZnO by XPS to further ensure that the change of contact angle is indeed due to the adsorption of $PC_{61}BM$ on TFTPA rather than contribution from the SAM or absorbed solvent since variation of contact angle can be affected by various sources. As can be seen from the results of the XPS measurements (Figure 3a), the peaks of fluorine binding energy F1s are around 688.2 and 689 eV for the ZnO substrates modified by TFTPA and PFBA, respectively, indicating the existence of SAM while pristine ZnO gives no signal of F1s. The integrated intensity of F1s of PFBA–ZnO is about twice that of TFTPA–ZnO. From the chemical structure of these two SAMs, the ratio of the fluorine atom number of PFBA to TFTPA is 5:4 or 1.25. However, the ratio of F1s intensity of PFBA to TFTPA is well

dx.doi.org/10.1021/am401430h | ACS Appl. Mater. Interfaces 2013, 5, 6665−6671

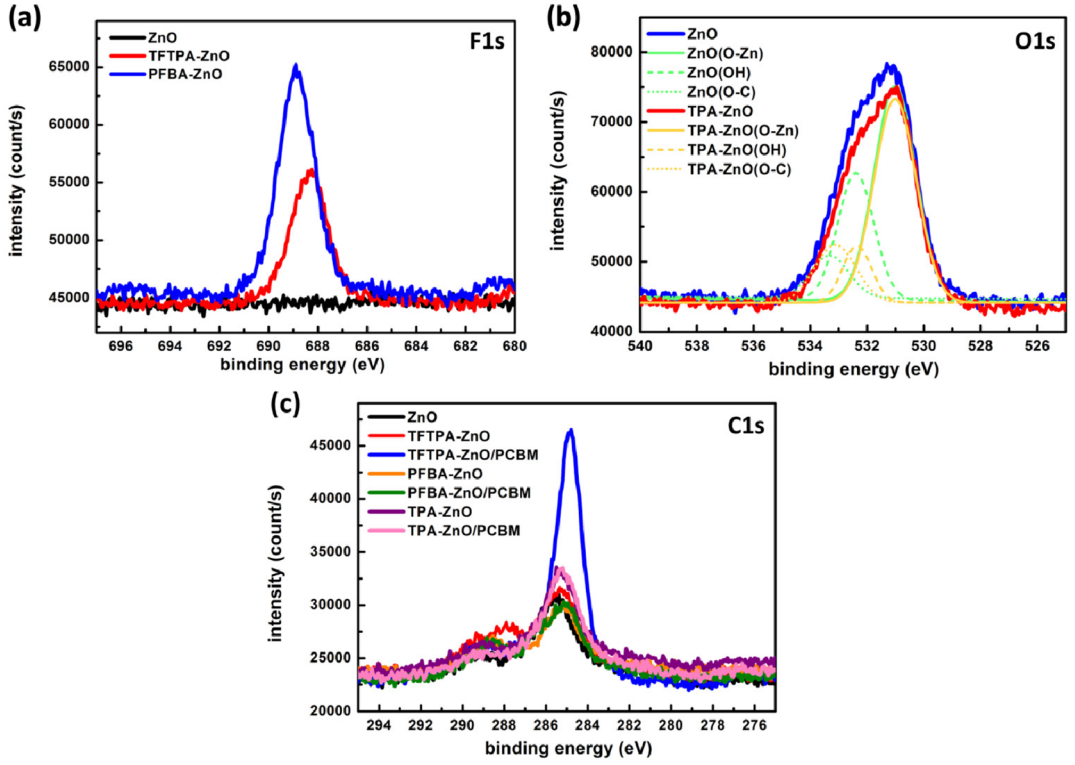

Figure 3. XPS spectra of ZnO without and with various treatments. (a) F1s signals from TFTPA−ZnO, PFBA−ZnO, and pristine ZnO; (b) O1s signal from TPA−ZnO and pristine ZnO; (c) C1s signals from TFTPA−, PFBA−, and TPA−ZnO and from those with additional $PC_{61}BM$ precoating.

Table 1. Device Performances without and with SAM Followed with and without $PC_{61}BM$ Precoating Process

active layer	SAM	J_{sc} [mA cm^{-2}]	V_{oc} [V]	FF [%]	PCE[d][%]	R_s [Ω cm^2]	R_{sh} [Ω cm^2]
P3HT:$PC_{61}BM$[a]	none	9.9	0.61	53	3.20 (3.20)	6.67	480
	TFTPA	10.6	0.59	59	3.70 (3.63)	2.08	1290
	TFTPA/$PC_{61}BM$	11.4	0.61	58	4.03 (4.01)	2.86	1307
	PFBA	10.6	0.61	57	3.69 (3.64)	6.76	1038
	PFBA/$PC_{61}BM$	10.6	0.59	59	3.69 (3.65)	3.445	1414
	TPA	10.6	0.59	57	3.56 (3.53)	4.00	1234
	TPA/$PC_{61}BM$	10.2	0.59	59	3.55 (3.54)	3.51	1315
P3HT:$PC_{71}BM$[b]	none	9.9	0.58	57	3.27 (3.22)	5.00	1188
	TFTPA/$PC_{71}BM$	11.8	0.59	58	4.04 (4.00)	4.35	1219
PTB7:$PC_{71}BM$[c]	none	12.5	0.72	67	6.03 (5.98)	0.38	10000
	TFTPA/$PC_{71}BM$	14.3	0.72	67	6.90 (6.85)	0.28	8695.7

[a]Device structure is ITO/ZnO + (SAM)/($PC_{61}BM$)/P3HT:$PC_{61}BM$/PEDOT:PSS/Ag. [b]Device structure is ITO/ZnO + (SAM)/($PC_{71}BM$)/P3HT:$PC_{71}BM$/PEDOT:PSS/Ag. [c]Device structure is ITO/ZnO + (SAM)/($PC_{71}BM$)/PTB7:$PC_{71}BM$/MoO3/Ag. [d]The listed PCE is the maximum value and that in the brackets is the average PCE from more than five devices

over the value 1.25, which is reasonable since the number of TFTPA molecules needed to cover the entire ZnO surface is about half of the number of PFBA molecules needed.[25] Therefore, the ratio of F1s intensity between PFBA and TFTPA should theoretically be 10:4 or 2.5, which is reasonably close to the experiment data (integrated area ratio of F1s of PFBA to TFTPA is about 2). This reflects that both −COOH groups in TFTPA could react with the −OH groups on ZnO and therefore a plane-on orientation is formed. The F1s peak shift between TFTPA and PFBA is probably because of the difference in number of carboxylate group and the difference in geometry between two materials. The O1s signal from ZnO (Figure 3b) can be deconvoluted into three peaks corresponding to the O−Zn bonding (531 eV), OH groups (532 eV), and the C−O species (533 eV).[36] The OH peak intensity decreases obviously after the SAM is deposited, which also indicates that TPA does bond onto the ZnO as the other two SAMs. However, the peak of 533 eV slightly increases and shifts toward lower binding energy by 0.2 eV. We infer that the increase and shift are attributed the carboxylate group on the TPA of which its O1s binding energy is slightly different from that of the C−O signal here. When $PC_{61}BM$ is adsorbed on TFPTA, the intensity of the carbon binding energy C1s should be stronger than the other cases, since $PC_{61}BM$ is primarily composed of carbon. From the C1s in Figure 3c, for all substrates, there are two peaks, one from the aromatic carbons, located at around 284.7−285.6 eV[26] and the other at higher binding energy from carboxyl or carboxylate side groups (around 288−289.4 eV).[26] The C1s peak of TFTPA−ZnO is slightly shifted to the lower binding energy which is similar to

dx.doi.org/10.1021/am401430h | ACS Appl. Mater. Interfaces 2013, 5, 6665−6671

the result reported previously.[35] We infer that the two electron donating O−(ZnO) group of TFPTA is responsible for the lower shift of carbon (in the carboxylate) signal. For the case of TFTPA−ZnO after treating with $PC_{61}BM$, its C1s peak at 284.7 eV is much stronger than those of the other substrates, which can be attributed to the carbons in C_{60}.[27] In fact, there are no significant changes on the other two SAMs (PFBA and TPA) after coating with $PC_{61}BM$. This XPS results clearly indicate that only TFTPA owns the capability to adsorb $PC_{61}BM$.

Device, External Quantum Efficiency (EQE), and Ultraviolet Photoelectron Spectroscopy (UPS). We apply the SAMs described above to i-PSC with the device structure ITO/SAM-ZnO/P3HT:$PC_{61}BM$/PEDOT:PSS/Ag under simulated 100 mW cm^{-2} AM 1.5 G illumination and their performance characteristic values are listed in Table 1. For the devices with modified ZnO (including TFTPA, PFBA, and TPA) but without preadsorption of $PC_{61}BM$, the current density enhances significantly from 9.9 mA cm^{-2}, for the pristine ZnO case, to 10.6 mA cm^{-2} for all the treated ZnO cases. The increase in current density in the same extent (0.7 mA cm^{-2}) in these three kinds of SAMs has no correlation with the contact angle and XPS results even though TFTPA is able to adsorb $PC_{61}BM$ effectively. This observation would indicate that the adsorption of $PC_{61}BM$ from the solution of P3HT:$PC_{61}BM$ during the spin-coating could be shielded by P3HT chains from direct contact with the substrate and thus the adsorption is insignificant. Therefore, the enhancement on current density here could be due to that the incorporation of the SAMs can effectively remove the hydroxyl group on ZnO surface, which is considered as an electron trap.[17] The obviously improved FF on the SAM-modified devices also contributes to the PCE enhancement. This can be attributed to the removal of the hydroxyl group on ZnO by depositing SAM that leads to a reduction of traps as reflected in the lowering of the series resistance and enhanced shunt resistance (Table 1.).

To overcome this ineffective adsorption during the direct coating of the active layer on the treated substrates indicates above, we then insert a layer of $PC_{61}BM$ alone by spin-coating from its solution in chlorobenzene (10 mg/mL) on the SAM-modified ZnO prior to coat an active layer on top of it for sufficient adsorption on TFTPA. The device structure with P3HT is ITO/SAM−ZnO/$PC_{61}BM$/P3HT:$PC_{61}BM$/PEDOT:PSS/Ag, and the corresponding performance parameter are listed in Table 1. The device with precoated $PC_{61}BM$ on TFTPA−ZnO further improves the PCE by 0.33% (from 3.70% to 4.03%), which is mainly resulted from the enhancement of current density by 0.8 mA cm^{-2} (from 10.6 to 11.4 mA cm^{-2}); while the devices with the precoated $PC_{61}BM$ on PFBA− and TPA−ZnO provide no improvement. Among the three devices with the precoating, the variations in V_{oc} and FF are insignificant, only within 3%. Here, it is assured that only TFTPA is capable to adsorb $PC_{61}BM$ and results in significant enhancement in electron collection. Therefore, a well-designed interface can effectively promote electron collection from the bulk and eliminate direct contacts of polymer chains in the active layer with ZnO and thus lower the probability of electron−hole recombination at the interface.

The EQE measurement shows the overall enhancement at both absorption ranges of P3HT (from 400 to 650 nm) and $PC_{61}BM$ (from 200 to 400 nm[4a]) (Figure 4b), which implies that the increase in current density is not due to the additional light-absorbing species, $PC_{61}BM$ adsorbed at the interface. If it really occurred, then the higher EQE would appear only at the shorter wavelength corresponding to the absorption of $PC_{61}BM$. However, the EQE at the range of P3HT absorption increases obviously, which strongly indicates that the $PC_{61}BM$ adsorbed on TFTPA−ZnO plays a role of facilitating electron collection from the bulk; otherwise, the EQE at the range of P3HT absorption would remain the same.

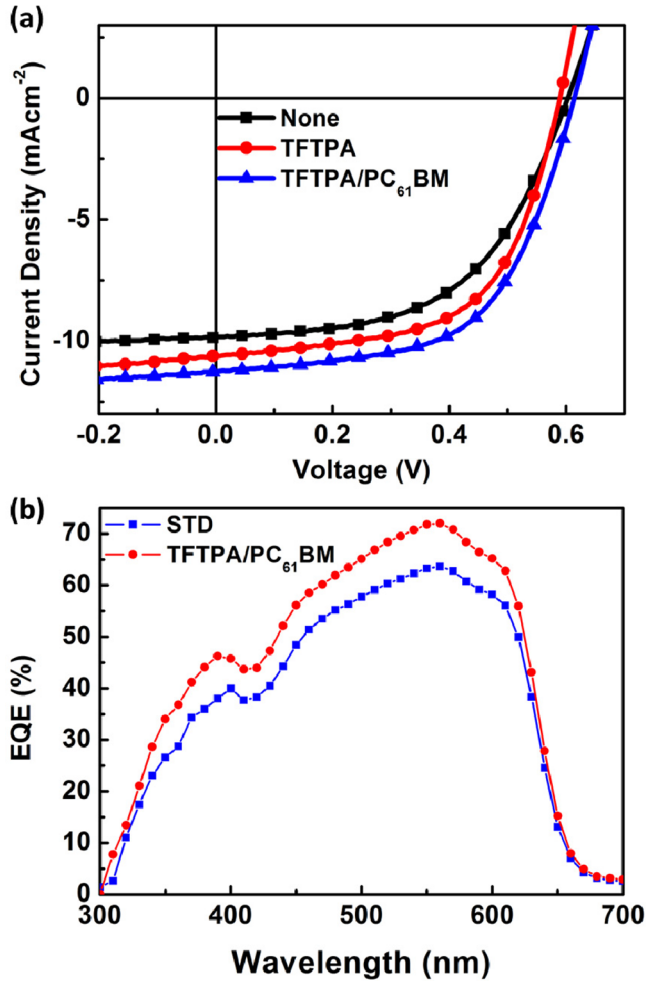

Figure 4. (a) $J-V$ curves of i-PSCs under simulated 100 mW cm^{-2} AM 1.5 G illumination with the device structure ITO/(TFTPA−ZnO)/($PC_{61}BM$)/P3HT:$PC_{61}BM$/PEDOT:PSS/Ag; (b) EQE spectra of the device ITO/ZnO/P3HT:$PC_{61}BM$/PEDOT:PSS/Ag which is designated as STD and of the device ITO/TFTPA−ZnO/$PC_{61}BM$/P3HT:$PC_{61}BM$/PEDOT:PSS/Ag which is designated as TFTPA/$PC_{61}BM$.

Furthermore, we measured the variation of energy levels of ZnO after the two successive modifications using UPS (Figure 5a and Table 2) and found that the TFTPA−ZnO keeps the same highest occupied molecular orbital (HOMO) level as the pristine ZnO (7.24 eV) indicating that TFTPA−ZnO does not affect the ionization potential of the ZnO surface. After $PC_{61}BM$ is adsorbed on the TFTPA−ZnO, the HOMO level decreases from 7.24 to 7.11 eV. Its lowest unoccupied molecular orbital (LUMO) can be calculated by adding up the bandgap obtained from the UV absorption spectra[22] directly on the HOMO level to give the LUMO levels of the pristine ZnO and TFTPA−ZnO 4.14 eV, while that after $PC_{61}BM$ treatment is 4.01 eV. The results imply that the adsorbed $PC_{61}BM$ forms an intermediate energy step at the

dx.doi.org/10.1021/am401430h | ACS Appl. Mater. Interfaces 2013, 5, 6665−6671

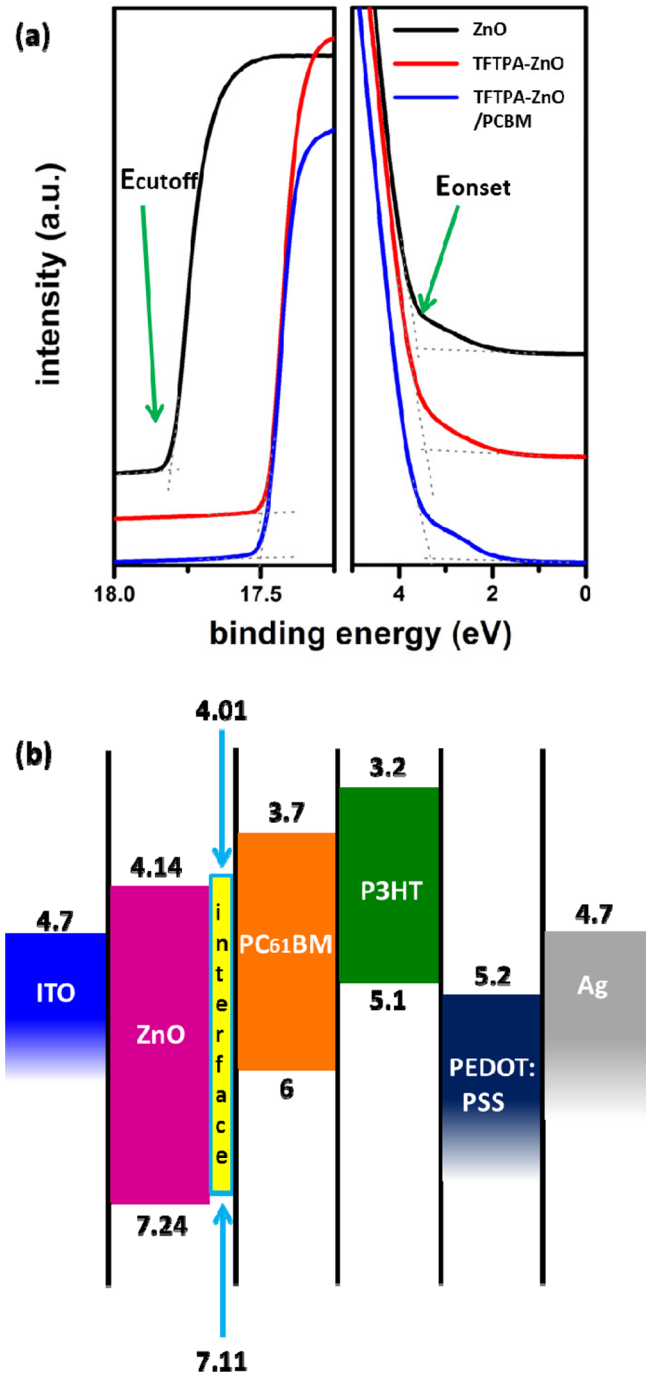

Figure 5. (a) UPS spectra of TFTPA-ZnO with $PC_{61}BM$ precoating; (b) Energy levels diagram of the materials in the devices, in which the yellow part (or designated as "interface") indicates the intermediate energy step created by the adsorption of $PC_{61}BM$ on the TFTPA–ZnO.

interface to facilitate the electron transport (Figure 5b). The presence of this intermediate step does highly correlate to the higher current density after the adsorbed $PC_{61}BM$ modification.

The concept of making a fullerene-rich interface by the TFTPA with its plane-on electron-depleted aromatic ring should be widely applicable to not only $PC_{61}BM$ but also other kinds of fullerene derivatives. We further choose $PC_{71}BM$ as the acceptor to confirm that TFTPA is also effective to other fullerene derivatives. The performances of the devices (Table 1) with the same structure as those for $PC_{61}BM$, ITO/

Table 2. Energy Levels of Pristine ZnO and TFTPA–ZnO without and with $PC_{61}BM$ Precoating

subtrate	E_{cutoff} (eV)	E_{onset} (eV)	HOMO (eV)[a]	LUMO (eV)[b]
ZnO	17.7	3.74	7.24	4.14
TFTPA–ZnO	17.5	3.54	7.24	4.14
TFTPA–ZnO/ $PC_{61}BM$	17.5	3.41	7.11	4.01

[a]The HOMO level is obtained from the UPS spectrum. [b]The LUMO level is obtained by adding the bandgap obtained from the UV–vis absorption spectrum to the HOMO level.[22]

TFTPA–ZnO/$PC_{71}BM$/P3HT:$PC_{71}BM$/PEDOT:PSS/Ag under simulated 100 mW cm^{-2} AM 1.5G illumination, as expected, show improvement in current density as for of the P3HT:$PC_{61}BM$ system devices. The current density increases from its original value 9.9 to 11.8 mAcm$-^{2}$, and the PCE also improves from 3.27% to 4.04%. The TFTPA–ZnO is able to adsorb the fullerene-derivatives via Coulombic interaction and thus form a fullerene-rich interface, and this interface should maintain its functionality when a different active polymer is coated on it. We further fabricate the devices with PTB7 as donor and $PC_{71}BM$ as acceptor under the same weight ratio with the device structure ITO/TFTPA-ZnO/$PC_{71}BM$/PTB7:$PC_{71}BM$/MoO3/Ag. The devices are under simulated 100 mW cm^{-2} AM 1.5 G illumination, and their performance characteristic values are listed in Table 1. Again, it shows that the $PC_{71}BM$ adsorption modification device presents higher current density (from 12.5 to 14.3 mA cm^{-2}) and the PCE increases significantly from 6.03% to 6.90%. Evidently, the capability of adsorbing fullerene derivatives onto the TFTPA–ZnO surface is applicable for different active polymers. Moreover, the adsorbed $PC_{71}BM$ layer does not interfere the original morphology of the active layer.

CONCLUSIONS

In conclusion, we present a simple and fast method to produce a fullerene-derivative-rich interface between active layer and ZnO in inverted polymer solar cell by incorporation of electron-poor TFTPA on the ZnO surface. Upon precoating a thin layer of fullerene derivative, it can adsorb onto the treated ZnO surface. The fullerene-rich interface can lower the electron/hole recombination probability and therefore facilitate the electron collection. The devices therefrom with P3HT or the low bandgap polymer PTB7 as donor and $PC_{61}BM$ or $PC_{71}BM$ as acceptor can lead to the increase in current density by 1.5 to 1.9 mA cm^{-2} and PCE by 0.77–0.87%, while V_{oc} and FF remain only a small variation within 3%. A remarkable enhancement on the power conversion efficiency was observed for the devices with the acceptor $PC_{61}BM$ (or $PC_{71}BM$) and the donor P3HT by promoting from 3.20% to 4.03% (or 3.27% to 4.04%) and for the system PTB7:$PC_{71}BM$ from 6.03% to 6.90%.

AUTHOR INFORMATION

Corresponding Author

*Tel.: 886-3-5710733. Fax: 886-3-5737798. E-mail: sachen@che.nthu.edu.tw.

Notes

The authors declare no competing financial interest.

■ ACKNOWLEDGMENTS

The authors thank the National Science Council for financial support through Project NSC-101-2120-M-007-004.

■ REFERENCES

(1) Yu, G.; Gao, J.; Hummelen, J. C.; Wudl, F.; Heeger, A. J. *Science* **1995**, *270*, 1789−1791.
(2) Ma, W.; Yang, C.; Gong, X.; Lee, K.; Heeger, A. J. *Adv. Funct. Mater.* **2005**, *15*, 1617−1622.
(3) He, Y.; Peng, B.; Zhao, G.; Zou, Y.; Li, Y. *J. Phys. Chem. C.* **2011**, *115*, 4340−4344.
(4) (a) He, Y.; Chen, H.-Y.; Hou, J.; Li, Y. *J. Am. Chem. Soc.* **2010**, *132*, 1377−1382. (b) Zhao, G.; He, Y.; Li, Y. *Adv. Mater.* **2010**, *22*, 4355−4358.
(5) Liang, Y.; Wu, Y.; Feng, D.; Tsai, S.-T.; Son, H.-J.; Li, G.; Yu, L. *J. Am. Chem. Soc.* **2009**, *131*, 56−57.
(6) Chen, H. Y.; Hou, J. H.; Zhang, S. Q.; Liang, Y. Y.; Yang, G. W.; Yang, Y.; Yu, L. P.; Wu, Y.; Li, G. *Nat. Photonics* **2009**, *3*, 649−653.
(7) Liang, Y.; Xu, Z.; Xia, J.; Tsai, S. T.; Wu, Y.; Li, G.; Ray, C.; Yu, L. *Adv. Mater.* **2010**, *22*, E135−E138.
(8) He, Z.; Zhong, C.; Huang, X.; Wong, W. -Y.; Wu, H.; Chen, L.; Su, S.; Cao, Y. *Adv. Mater.* **2011**, *23*, 4636−4643.
(9) Liao, S.-H.; Li, Y.-L.; Jen, T.-Z.; Cheng, Y.-S.; Chen, S.-A. *J. Am. Chem. Soc.* **2012**, *134*, 14271.
(10) Krebs, F. C.; Norrman, K. *Progr. Photovolt.: Res. Appl.* **2007**, *15*, 697−712.
(11) Li, G.; Chu, C. W.; Shrotriya, V.; Huang, J.; Yang, Y. *Appl. Phys. Lett.* **2006**, *88*, 253503.
(12) Hau, S. K.; Yip, H. L.; Baek, N. S.; Zou, J.; O'Malley, K.; Jen, A. K. Y. *Appl. Phys. Lett.* **2008**, *92* (253301), 1−3.
(13) (a) Hau, S. K.; Yip, H. L.; Acton, O.; Baek, N. S.; Ma, H.; Jen, A. K. Y. *J. Mater. Chem.* **2008**, *18*, 5113−5119. (b) Hau, S. K.; Yip, H. -L.; Ma, H.; Jen, Alex K.-Y. *Appl. Phys. Lett.* **2008**, *93* (233304), 1−3.
(14) Waldauf, C.; Morana, M.; Denk, P.; Schilinsky, P.; Coakley, K.; Choulis, S. A.; Brabec, C. J. *Appl. Phys. Lett.* **2006**, *89* (233517), 1−3.
(15) Hsieh, C.-H.; Cheng, Y.-J.; Li, P.-J.; Chen, C.-H.; Dubosc, M.; Liang, R.-M.; Hsu, C.-S. *J. Am. Chem. Soc.* **2010**, *132*, 4887−4893.
(16) Jung, J. W.; Jo, J. W.; Jo, W. H. *Adv. Mater.* **2011**, *23*, 1782−1787.
(17) Hau, S. K.; Cheng, Y.-J.; Yip, H.-L.; Zhang, Y.; Ma, H.; Jen, A. K. Y. *Appl. Mater. Interfaces* **2010**, *2*, 1892−1902.
(18) Schneider, H.; Vogelhuber, K. M.; Schinle, F.; Weber, J. M. *J. Am. Chem. Soc.* **2007**, *129*, 13022−13026.
(19) Meyer, E. A.; Castellano, R. K.; Diederich, F. *Angew. Chem., Int. Ed.* **2003**, *42*, 1210−1250.
(20) Okamoto, T.; Nakahara, K.; Saeki, A.; Seki, S.; Oh, J. H.; Akkerman, H. B.; Bao, Z.; Matsuo, Y. *Chem. Mater.* **2011**, *23*, 1646−1649.
(21) Li, C. −Z.; Matsuo, Y.; Niinomi, T.; Satoac, Y.; Nakamura, E. *Chem. Commun.* **2010**, *46*, 8582−8584.
(22) Maensiri, S.; Laokul, P.; Promarak, V. *J. Cryst. Growth* **2006**, *289*, 102−106.
(23) Sun, Y.; Seo, J. H.; Takacs, C. J.; Seifter, J.; Heeger, A. J. *Adv. Mater.* **2011**, *23*, 1679−1683.
(24) Kalyanasundaram, K.; Gratzel, M. *Coord. Chem. Rev.* **1998**, *77*, 347−414.
(25) Moser, J.; Punchihewa, S.; Infelta, P. P.; Gratzel, M. *Langmuir* **1991**, *7*, 3012−3018.
(26) Stepanow, S.; Strunskus, T.; Lingenfelder, M.; Dmitriev, A.; Spillmann, H.; Lin, N.; Barth, J. V.; Wo1ll, Ch.; Kern, K. *J. Phys. Chem. B* **2004**, *108*, 19392−19397.
(27) Mitsumoto, R.; Araki, T.; Ito, E.; Ouchi, Y.; Seki, K.; Kikuchi, K.; Achiba, Y.; Kurosaki, H.; Sonoda, T.; Kobayashi, H.; Boltalina, O. V.; Pavlovich, V. K.; Sidorov, L. N.; Hattori, Y.; Liu, N.; Yajima, S.; Kawasaki, S.; Okino, F.; Touhara, H. *J. Phys. Chem. A* **1998**, *102*, 552−560.
(28) Li, Y. *Acc. Chem. Res.* **2012**, *45* (5), 723−733.
(29) Guo, X.; Zhang, M.; Tan, J.; Zhang, S.; Huo, L.; Hu, W.; Li, Y.; Hou, J. *Adv. Mater.* **2012**, *24*, 6536−6541.
(30) Huo, L.; Zhang, S.; Guo, X.; Xu, F.; Li, Y.; Hou, J. *Angew. Chem., Int. Ed.* **2011**, *50*, 9697−9702.
(31) Tan, Z.; Zhang, W.; Zhang, Z.; Qian, D.; Huang, Y.; Hou, J.; Li, Y. *Adv. Mater.* **2012**, *24*, 1476−1481.
(32) Sun, Y.; Seo, J. H.; Takacs, C. J.; Seifter, J.; Heeger, A. J. *Adv. Mater.* **2011**, *23*, 1679−1683.
(33) Li, X.; Choy, W. C. H.; Huo, L.; Xie, F.; Sha, W. E. I.; Ding, B.; Guo, X.; Li, Y.; Hou, J.; You, J.; Yang, Y. *Adv. Mater.* **2012**, *24*, 3046−3052.
(34) Liang, Z.; Zhang, Q.; Wiranwetchayan, O.; Xi, J.; Yang, Z.; Park, K.; Li, C.; Cao, G. *Adv. Funct. Mater.* **2012**, *22*, 2194−2201.
(35) Paniagua, S. A.; Hotchkiss, P. J.; Jones, S. C.; Marder, S. R.; Mudalige, A.; Marrikar, F. S.; Pemberton, J. E.; Armstrong, N. R. *J. Phys. Chem. C* **2008**, *112*, 7809−7817.
(36) (a) Ballerini, G.; Ogle, K.; B. -Labrousse, M.-G. *Appl. Surf. Sci.* **2007**, *253*, 6860−6867. (b) Mu, J.; Shao, C.; Guo, Z.; Zhang, Z.; Zhang, M.; Zhang, P.; Chen, B.; Liu, Y. *ACS Appl. Mater. Interfaces* **2011**, *3*, 590−596.